A Fault Tolerant Machine Drive Based on Permanent Magnet Assisted Synchronous Reluctance Machine

Bo Wang, *Member IEEE*, Jiabin Wang, *Senior Member, IEEE*, Bhaskar Sen, *Member IEEE*, Antonio Griffo, *Member IEEE*, Zhigang Sun, and Ellis Chong

Abstract —A fault tolerant machine drive based on permanent magnet assisted synchronous reluctance machine (PMA SynRM) is proposed and investigated for aerospace applications where reliability and safety are crucial. In order to achieve enhanced fault tolerant capability, the risk of permanent magnet field that cannot be turned off under fault conditions is minimized without compromise in torque density and efficiency. This is achieved by employing a synchronous reluctance rotor topology with embedded permanent magnets. Three independent, segregated 3-phase windings are configured to ensure isolation and non-overlapping between the three 3-phase winding sets. Each 3-phase winding set is driven by a standard 3-phase inverter to facilitate fast integration and cost reduction. The machine behavior under various fault conditions has been evaluated by finite element (FE) simulations. A 40kW prototype was designed, constructed and tested. The test results demonstrate the performance and excellent fault tolerant capability of the proposed drive system under various faults, including open circuit and short circuit conditions.

Index Terms—Fault tolerant machine, permanent magnet assisted synchronous reluctance machine, multi-phase machine, non-overlapped winding configuration.

I. INTRODUCTION

FAULT tolerant machine and drives are capable of providing uninterrupted operation during fault conditions, therefore being attractive in safety critical applications, such as aerospace and electric traction [1, 2]. While electrical drives possess enhanced functionality, adaptability and controllability compared with conventional mechanical, hydraulic, and pneumatic driven systems [3], relative low reliability of electric drive systems restricts their wide applications since an unexpected fault would cause serious consequences or economic losses. Thus, fault tolerance is an essential requirement for electrical drives to attain high availability in safety critical applications.

To this end, various fault tolerant machine topologies and techniques have been investigated in literatures. The most straightforward approach is to adopt two or more machine-drive modules either in series or in parallel [4, 5]. However, use of multiple machine drives for redundant operation occupies large space and necessitates additional accessories to guarantee its operation in healthy and fault conditions, resulting in low power density and bulky size. Alternatively, fault tolerance may be achieved on a single 3-phase machine by employing a neutral connection to the midpoint of the DC link or to a fourth inverter leg [6]. Zero sequence current is utilized to generate the equivalent rotating magneto-motive force (MMF) if one phase is open-circuited. The neutral connection can be eliminated by employing more than three phases in a single machine [7, 8]. Depending on the number of phases, a multi-phase (number of phases>3) machine may be capable of continuous operation when one or more than one phase has failed. The concept has been realized in both induction machines and PM machines [9-13]. Additionally, various control algorithms have been proposed to achieve the maximum attainable torque, or minimum torque ripple [14-17] under fault conditions. It is worth noting that the majorities of the above measures address the open circuit failure only.

In order to accommodate short circuit failure in the phase windings or switches, advanced fault tolerant drives were developed. Owing to its rugged, magnet-free rotor structure and concentrated windings, switched reluctance machine (SRM) is inherently fault tolerant [18, 19]. Each phase winding is magnetically, thermally and electrically isolated. Due to low mutual coupling between phases, the short circuit current as a result of inverter or winding failure can be limited in a safe region [20]. However, an SRM exhibits high torque ripple, undesirable noise and vibration, and inferior torque density/efficiency.

In [21] a single layer fractional slot concentrated winding (FSCW) permanent machine is developed that facilitates electrical, magnetic, thermal, and physical isolations between phases. The slot geometry is specially designed to obtain per-unit inductance. As a result, the terminal short circuit current is limited under the rated value. This methodology has also been extended to switched flux PM machines [22]. However, due to the concentrated windings, very little reluctance torque can be exploited in this type of machine. The output torque of a FSCW PM machine purely relies on the PM field and, consequently, increase in torque capability leads to higher flux linkage. The presence of strong PM field poses a safety hazard to the machine as it cannot be turned off in the event of a fault [23]. The back electromotive force (emf) may be higher than the DC link voltage at high speeds and uncontrolled rectification via the diodes may occur in case of an inverter failure. Excessive regenerative power which flows to the DC link capacitor may cause catastrophic failure to the drive system. Significant braking torque may also be imposed on the rotor causing

excessive stress to the mechanical system or sudden reduction in speed which may induce accidents in traction drives. Thus, the maximum back emf should be limited [24]. However, this is in conflict with the requirements for torque production. It can be shown that if the FSCW machine with limited maximum back-emf is required to operate in a wide constant power range, the VA rating of the inverter increases linearly with the speed, which in turn increases the overall size and cost of the drive. Further, the use of concentric windings also gives rise to sub- and high-order MMF space harmonics which produce extra rotor loss. Hence, the magnets need to be segmented axially or circumferentially to avoid excessive rotor temperature [25].

Recently, PMA SynRM has gained increasing interests as a viable candidate for electric traction due to reduced magnets usage, extended field weakening range and comparable performance with conventional PM machines [26, 27]. These unique characteristics are mainly attributed to the combined torque production mechanism, both the PM torque and reluctance torque. The reluctance torque enables use of less magnet material and results in low back emf which improves the machine's fault tolerant capability. However the distributed overlapping windings used in this type of machines yield strong inter-phase coupling and physical contacts between the coils in different phases. Consequently, a fault in one phase may propagate to or affect other phases. For a conventional 3-phase machine drive, a single failure in any part of the drive will lead to a complete failure [28-30].

This paper aims to develop a new fault tolerant machine drive based on PMA SynRM topology for aerospace application. By employing appropriate winding configuration, the machine can be optimized to have high torque density while exhibiting excellent fault tolerant characteristics. Detailed analysis has been conducted to assess its performance under healthy and various fault conditions. A 40kW prototype was designed and built to evaluate the torque capabilities under various operating conditions. Extensive experimental tests have been performed to validate the fault tolerant capability of the proposed machine drive.

II. FAULT TOLERANT WINDING CONFIGURATION FOR PMA SYNRM

Conventional 3-phase windings of a PMA SynRM are usually distributed as shown in Fig. 1 in order to produce a nearly sinusoidal MMF in the air gap albeit they are not conducive to fault tolerance. It is possible to configure the windings as three isolated 3-phase sets for the purpose of triple redundancy. However, the windings of different sets are overlapped and bundled together which is prone to inter-phase short circuits. Strong magnetic coupling also exists between different 3-phase sets. In addition, the heat produced by a faulty 3-phase set may spread to the other healthy sets via the overlapped windings.

In order to achieve physical, electrical and thermal isolations to provide enhanced fault tolerance for the PMA SynRM, a segregated triple-redundant 3-phase winding configuration is proposed as shown in Fig. 2 [31]. The conventional overlapped

windings are divided into three separate 3-phase winding sets so that there is no contact between them, resulting in physical and thermal isolation. The electrical isolation is achieved by using three standard inverters to drive each 3-phase set.

According to Fig. 2, the "go" and "return" positions of the coils in phases C, F and I are reversed whilst the induced voltages in phases C, F and I are unchanged owing to the periodic airgap flux density distribution. As a result, each winding set ABC, DEF and GHI still forms a balanced 3-phase winding. Since the currents in the slots are not affected by the new winding configuration, the MMF distribution and the performance of the machine in healthy conditions are exactly the same as the original one shown in Fig. 1. Thus, all the merits of the PMA SynRM, such as reduced magnet usage, low back emf, inherent large reluctance torque, high efficiency and high torque density are maintained. Most importantly, the segregated windings and independent inverters lead to excellent fault tolerance since the risk of fault propagation between different 3-phase winding sets is minimized and the three independent modules provide redundancy for various faults [32]. It should be noted that the mutual coupling due to end winding leakage flux of the proposed windings will have slight asymmetry. However, this leakage flux is very small, and the effect of the asymmetry is negligible.
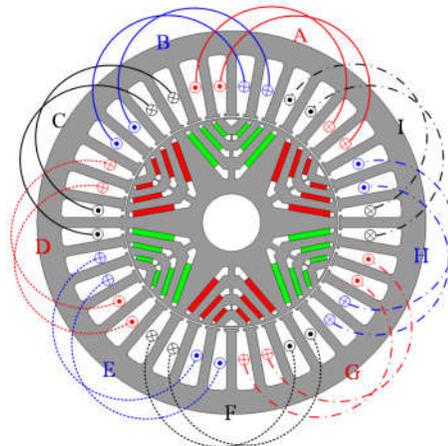

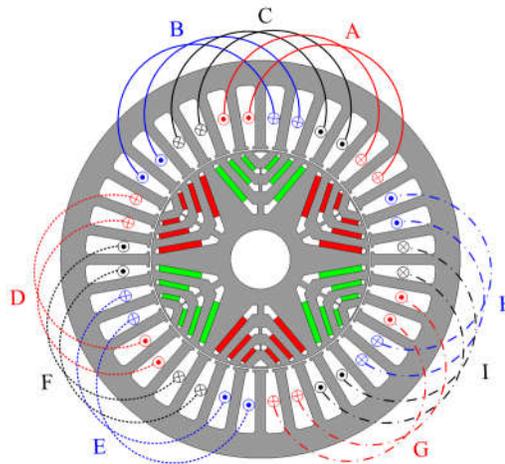Fig. 1. PMA SynRM with conventional overlapped windings.

Fig. 2. PMA SynRM with proposed segregated windings.

For this type of machine, in case of an open-circuit fault in

an inverter switch or the windings, the faulty 3-phase winding set can be simply deactivated by opening all the switches in that set, and the remaining two healthy 3-phase sets are capable of continuous operation, with about one third reduction in output torque or power. If a short circuit failure occurs in an inverter switch or in one 3-phase winding, a terminal short circuit can be applied to the faulty set by closing the three bottom or top switches of the corresponding 3-phase inverter. Since the PM flux in the machine is quite low, the short circuit currents will be limited below the rated value. Thus, owing to the winding separation, a fault in one 3-phase system can be isolated and the other two sets can continue operation to deliver torque or power.

It follows that the PMA SynRM with the segregated winding configuration exhibits good performance as well as excellent fault tolerance. The segregated windings are realized with no penalties and no additional cost. Only a winding reconfiguration is required to form multiple 3-phase winding sets and each 3-phase set is driven by a standard 3-phase inverter. Separating a 3-phase winding into multiple 3-phase sets reduces the currents in each 3-phase set, spreading heat more evenly in the inverter switches and hence facilitating machine-inverter integrations, particularly for high power drives. Although the proposed winding segregation is primarily aimed for PMA SynRM, it is also applicable to the other machines with distributed windings to enhance the fault tolerance, such as synchronous reluctance machines, surface mounted PM machines, synchronous wound field machines and induction machines [33]. The number of 3-phase modules can be selected according to application requirements. It should be noted that while the proposed winding segregation is not new [34], its exploitation in PMA SynRM to achieve desirable fault tolerance has not been reported and demonstrated in literature to date.

III. PROTOTYPE DESIGN

A prototype machine has been designed to assess the performance of the proposed fault tolerant machine against the design specifications given in Table I. The stator and rotor cores employ 0.2mm Cobalt-iron lamination [35]. The magnets are Vacomax 225HR whose remanence is 1.1T. This material is selected for its ability to operate at very high temperature and its insensitivity to temperature variation. Oil cooling is chosen to enhance torque density. The machine requires a wide constant power operation range from 4000rpm to 19200rpm and the PMA SynRM is particular suitable for deep field weakening owing to its low characteristic current I_{ch} defined as the ratio of PM flux linkage φ_m to the d-axis inductance L_d in (1).

$$I_{ch} = \varphi_m/L_d \tag{1}$$

To address the redundancy requirement, triple 3-phase modules offer a good compromise between the fault tolerance and overall complexity. Thus, a PMA SynRM with 36 slots and 6 poles was selected for the design study.

Compared with a conventional 3-phase PMA SynRM, only

the windings are reconfigured. Hence, the machine can be designed as a conventional 3-phase machine by exploiting its periodicity. 1/6 of the machine geometry was used in FE based design optimization process as shown in Fig. 3. The torque was evaluated as in (2) where p is pole-pair number, φ_d, φ_q and i_d, i_q are the flux linkages and currents in d, q axes, respectively.

$$T = 1.5p(\varphi_d i_q - \varphi_q i_d) \tag{2}$$

Table I
DESIGN SPECIFICATIONS OF THE MACHINE

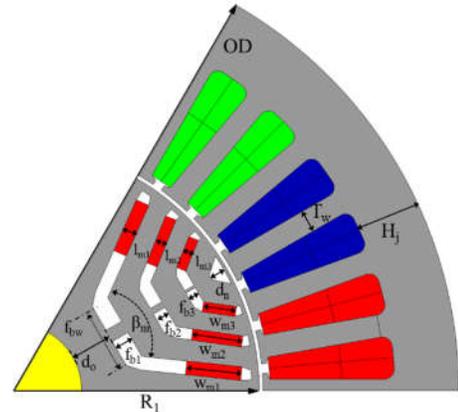| Specification	Symbol	Value
Base speed	ω_b	4000rpm
Maximum speed	ω_m	19200rpm
Rated power	P_r	40kW
Peak power	P_p	50kW
Rated torque at base speed	T_r	95.5Nm
Rated torque at maximum speed	T_{rm}	19.9Nm
Nominal DC link voltage	V_{dc}	270V
Rated current (peak)	I_r	120A
Characteristic current (peak)	I_{ch}	<80A
Maximum inverter current (peak)	I_{max}	200A
Ambient temperature	T_{amb}	100℃
Maximum winding temperature	Tw_m	180℃
Cooling medium	-	Aeroshell oil
Redundancy	1	Triple or quadruple

Fig. 3. Optimization geometry parameters of PMA SynRM.

The multiple embedded layers and cutout in the rotor lead to enhanced reluctance torque production capability, whilst ensuring good structural integrity and manufacturability of the rotor. The magnets in the rotor are placed on the sides of the rotor flux barriers. This topology is conducive to reduction of the magnet usage for a given PM flux linkage compared with other magnet configurations (e.g. single blocks in the middle of the flux barriers or a combination of middle and side blocks in the flux barriers). This can be attributed to the flux-focusing effect which enhances the flux in the airgap. In addition, the magnets are placed closer to the airgap leading to less flux leakage [36].

The geometry parameters to be optimized are shown in Fig. 3. The machine has been optimized against the design specifications, thermal and mechanical constrains to maximize the efficiency at the base speed rated torque operation point using the FE based technique as described in [37]. The fault tolerance of the machine was examined after the optimization, some fine tuning was conducted to satisfy the various objectives

and constraints listed in Table I. The final optimized design parameters are listed in Table II.

Table II
OPTIMIZED DESIGN PARAMETERS

Parameter	Symbol	Value
Stator radius	R_s	90mm
Back iron thickness	H_j	10.25mm
Tooth width	T_w	5.1mm
Rotor radius	R_I	51.75mm
Magnet thickness	l_{mI}	2.8mm
Magnet width	w_{mI}	14.88mm
Middle flux barrier thickness	f_{bI}	2.9mm
Middle flux barrier width	f_{bw}	10.64mm
Magnet layer's angular span	β_m	157.6°
Magnet layer's depth	d_0	9.83mm
Turn number per coil	TN	8

IV. PERFORMANCE EVALUATION

In this section, the performance of the optimized machine at healthy condition is evaluated and its fault tolerance to various faults is also examined via FE simulations. All the evaluations are conducted at the base speed of 4000rpm unless otherwise stated. In addition, without loss of generality, the faults, including open- and short-circuit faults, are assumed to occur in the ABC 3-phase winding set.

A. Back Emf

Initially, the machine under no load condition was evaluated. The phase flux linkages and back-emfs are shown in Fig. 4 and Fig. 5, respectively. Since the flux linkages and back-emfs in all three 3-phase sets are identical, only the waveforms for set ABC are shown. It is observed that the PM flux linkages and back emfs are relatively low and the characteristic current I_{ch} is evaluated as 75.3A which is much lower than the rated value. This means that in case of a terminal short circuit, no excessive currents would be induced, and the resultant heat could be easily dissipated by the oil cooling system. Further, it can be deduced that the peak value of line-to-line back emf at the maximum speed is 273V, which will have benign effect in the event of inverter failure.
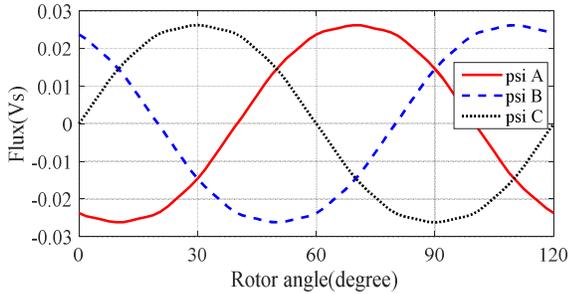

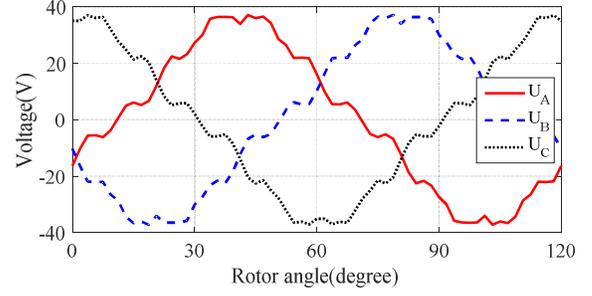Fig. 4. Phase flux linkages in no load condition.

Fig. 5. Back emf at 4000 rpm.

B. Healthy Operation

With 118.5A current excitation, the optimal γ angle between the q-axis and the current vector for maximum torque per Ampere (MTPA) is evaluated as 52°. The resultant torque waveform at the rated power of 40kW is shown in Fig. 6. The machine outputs an average torque of 95.5Nm. The torque ripple is evaluated as 16.8% which is mainly due to the 6th and 12th harmonic produced by the interaction of the rotor saliency and stator slotting. The PM torque and reluctance torque account 30% and 70%, respectively [38]. Although the PM flux is relatively low, the machine still achieves high torque density since 70% of the torque is produced by the reluctance component.
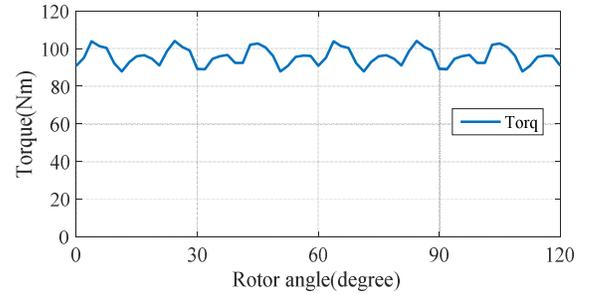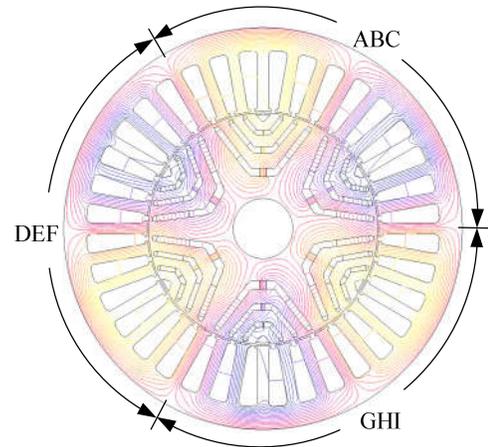

Fig. 6. Torque in healthy condition.

Fig. 7. Flux distribution in healthy condition.

Fig. 7 shows the 2D flux distribution under rated conditions. It is evident the distribution repeats 3 times periodically over 360 degrees. Thus, the flux linkages of the three 3-phase sets are also identical under healthy conditions. By way of example, Fig. 8 shows the flux linkage waveforms of set ABC. While

distortions due to space harmonics and magnetic saturation are visible, the waveforms exhibit the 3-phase symmetry.
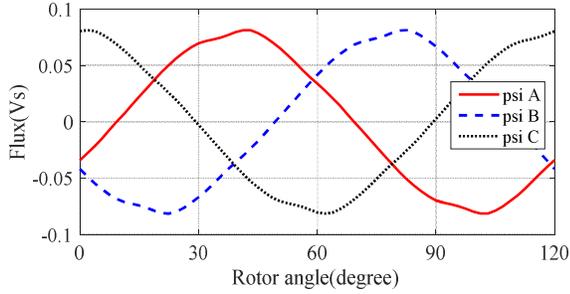

Fig. 8. Phase flux linkages in healthy condition.

C. One Set Open Circuit

In case of a winding open circuit, switch open-circuit failure or control failures, the faulty set of 3-phase winding should be deactivated by opening all the inverter switches. The currents in the faulty set become zero, leading to one set open-circuit failure mode. The remaining two 3-phase sets are excited by the same currents and the resulting torque waveform is shown in Fig. 9. The average torque of the machine in this condition is 54.6Nm. Thus, the open circuit torque capability ρ_{oc}, defined as the percentage ratio of open circuit torque, T_{oc} to the rated torque T_r, can be calculated as:

$$\rho_{oc} = T_{oc}/T_r \times 100\% = 57\%. \tag{3}$$

The torque reduction is slightly higher than 1/3 pu. Given that the thermal load under this condition is much reduced due to one set being open circuited, the currents in the remaining two healthy 3-phase sets can be increased to offset the torque reduction to obtain 2/3pu torque. The torque ripple under the open circuit condition is 16.1%. In addition to the 6th and 12th harmonic torque ripples, a 2nd harmonic torque ripple is clearly visible in the torque waveform. This is caused by the electromagnetic unbalance resulting from the open-circuit fault which is evident from the flux distribution shown in Fig. 10 under the open circuit condition of the ABC set.
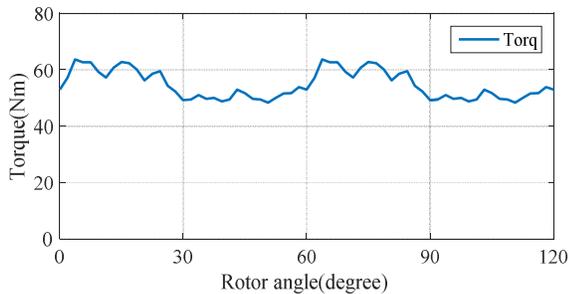

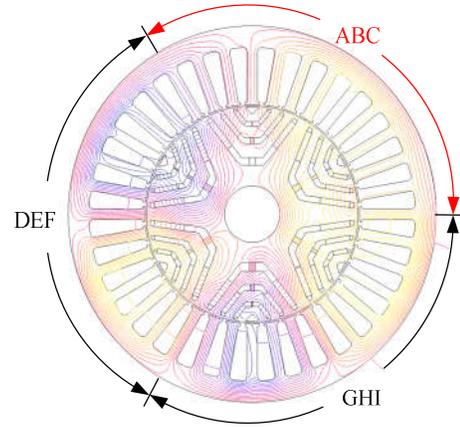Fig. 9. Torque with set ABC open circuited.

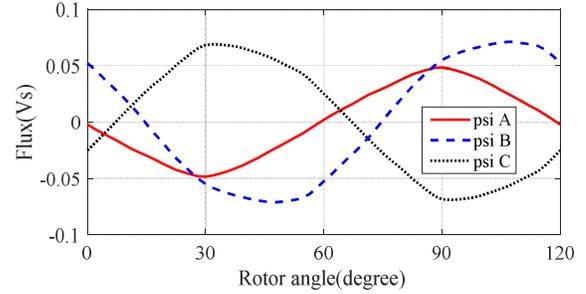Fig. 10. Flux distribution with set ABC open circuited.

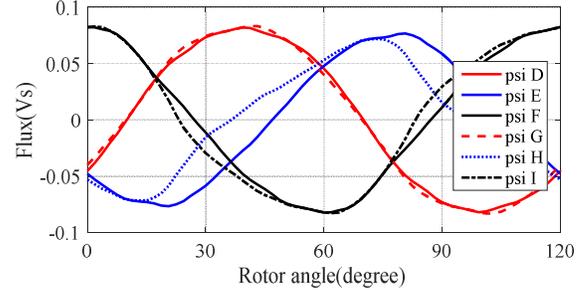Fig. 11. Faulty phase flux linkages with set ABC open circuited.

Fig. 12. Healthy phase flux linkages with set ABC open circuited.

As shown in Fig. 11, the phase flux linkages in the open-circuited ABC set are heavily distorted from the no load PM flux. This indicates that mutual coupling still exists in the three 3-phase winding sets of the machine. In fact, although the currents of the fault set are zero, the currents in the other two healthy sets will produce a nonzero MMF over the fault set region. Hence, the distorted flux linkages are the combined effect of the rotor magnets and currents in the other two healthy sets.

Similarly, the flux linkage waveforms of the healthy DEF and GHI sets shown in Fig. 12 are no longer balanced though they are still excited by sinusoidal currents. The amount of distortion in the flux linkage waveforms due to the unbalance is different in each phase. The distortions in phases D, F, G and I are relatively small while more distortions are noticed in phases E and H. This may be attributed to local saturation caused by asymmetrical MMF distribution.

D. One Set Short Circuit

If a switch in the inverter or the phase winding is short-circuited, that particular inverter should turn-on all its top or bottom switches to create a terminal short circuit for the faulty 3-phase set. The healthy sets are still excited by the inverter for continuous operation similarly to the case of open-circuit fault. The resultant short-circuit phase currents are shown in Fig. 13 and their root-mean-square (RMS) values are much lower than the rated current since the PM flux in the machine is relatively low. Hence, no excessive heat will be produced in the faulty set and the machine will be safe to continue its operation. Such low short-circuit current is an inherent property of this type of machine and no penalty like the small slot opening is required in the machine design to achieve this advantage. It is observed that the short circuit phase currents are asymmetrical. Again, this is attributed to the mutual coupling between the healthy sets and the faulty set since they are not completely magnetically isolated.
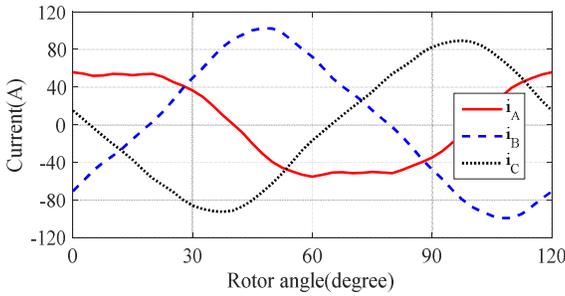

Fig. 13. Short circuit phase currents.

The flux distribution under the short circuit condition is shown in Fig. 14. As can be seen, the flux in the region occupied by the short-circuited ABC set is almost nullified by the short-circuit currents. The flux density in this region is quite low. The resultant flux linkage waveforms of the fault set are plotted in Fig. 15. It is evident that the flux linkages are much lower than those in the healthy condition. The remaining flux linkages consist of mainly zero sequence components since there is no zero sequence currents in the star connected 3-phase winding to nullify them. It is also seen that phase B exhibits the highest flux linkage which is consistent with the highest phase current shown in Fig. 13. In contrast, the flux density distribution in set DEF and GHI regions is almost normal as is evident from the flux linkage waveforms shown in Fig. 16.

The torque waveform under the short circuit condition is plotted in Fig. 17 where the average torque and torque ripple are 63.5Nm and 12.4%, respectively. The short circuit torque capability ρ_{sc} is evaluated to be 66%, very close to two thirds of the rated and slightly higher than that in the open circuit case. The torque ripple is lower than the open circuit case and contains mainly the 2nd and 12th harmonics. These results confirm that the short-circuit fault can be accommodated by the proposed machine.
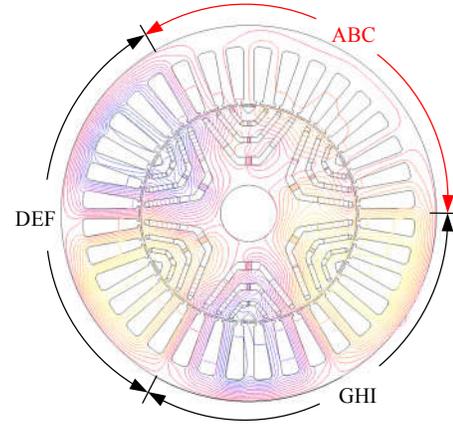

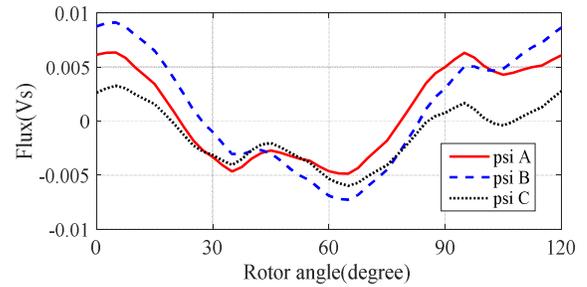Fig. 14. Flux distribution with set ABC short circuited.

Fig. 15. Faulty phase flux linkages with set ABC short circuited.
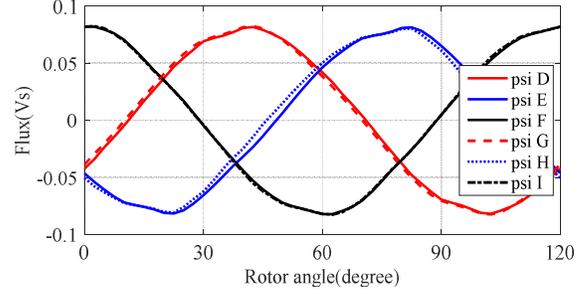

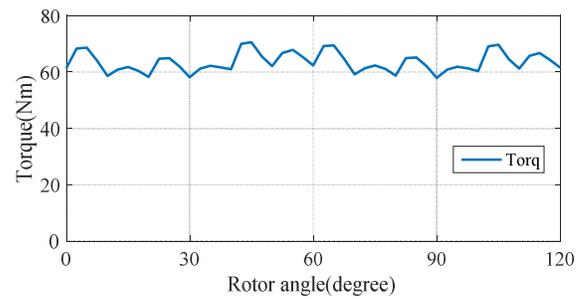Fig. 16. Healthy phase flux linkages with set ABC short circuited.

Fig. 17. Torque with set ABC short circuited.

It should be noted that the worst fault condition is a single turn short circuit which takes place in the turn close to the slot opening and the resulting short-circuit current is ~9pu. Application of terminal short circuit can significantly reduce this current as a remedy action. Extensive FE analyses were performed to identify the location of the turn with the largest short current after the remedy action. It is found that for motoring operation, the single turn short circuit with the largest current occurs in the trailing slot (the last slot in the direction of

rotation) of a 3-phase set whilst in generating mode, the worst case occurs in the leading slot (the first slot in the direction of rotation). After applying the terminal short circuit, the resultant turn fault current is reduced to 3.2pu. Since the short circuit current in the healthy turns of the 3-phase set is much lower than the rated as shown in Fig. 13, the overall thermal loading under the worst case does not lead to excessive temperature rise. The output torque under the condition with the remedy action is similar to that shown in Fig. 17.

V. PROTOTYPING AND EXPERIMENTAL TEST

A machine prototype has been constructed based on the optimal design given in Table II. In order to reduce the torque ripple and voltage harmonics, the stator lamination has been skewed by one slot, i.e. 10 degree. The stator and rotor stack are shown in Fig. 18(a) and (b), respectively. The key feature of the proposed machine is the segregated windings as shown in Fig. 18(c). It can be seen that no physical contact exists between the three sets of windings. The windings are further protected by Stycast potting to improve the thermal dissipation as shown in Fig. 18(d). Oil cooling channels as shown in Fig. 18(e), are embedded in the stator housing, and the completed machine assembly with the oil inlet and outlet is shown in Fig. 18(f).
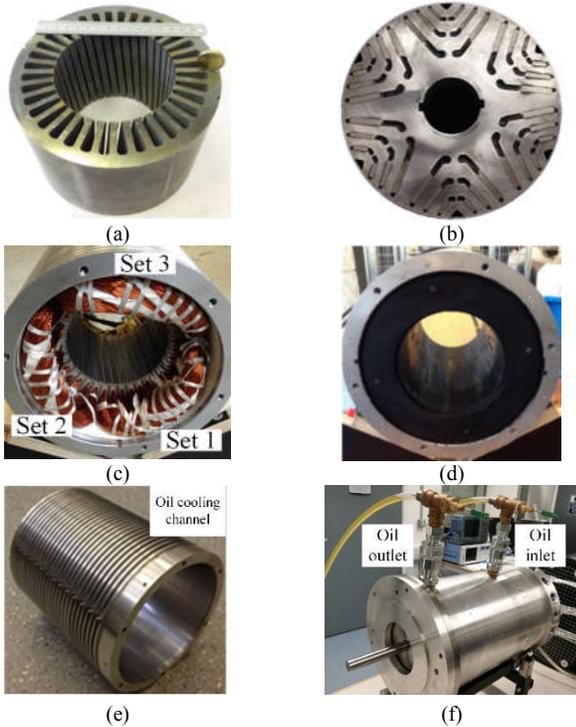

Fig. 18. Machine prototype (a) Skewed stator stack (b) Rotor stack with magnets (c) Segregated winding (d) Stycast potted winding (e) Oil cooling jacket (f) Machine assembly.
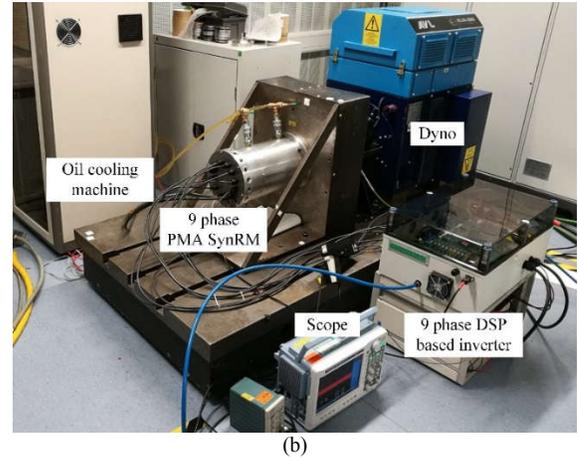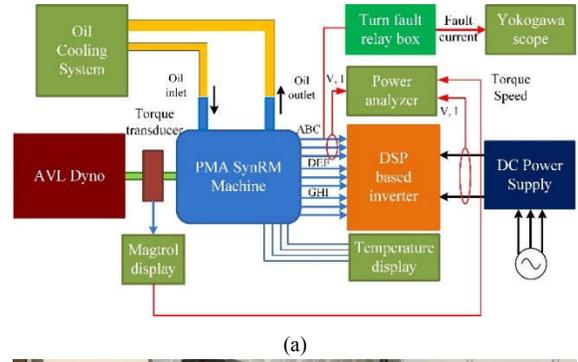

Fig. 19 Test bench illustration (a) Schematic test configuration (b) Test rig.

Fig. 19 shows the schematic test configuration and the photo of test rig respectively. The machine is mounted on the test rig and connected to the dynamometer via a high precision in-line torque transducer. A 9-phase inverter, configured as three independent 3-phase sets has also been developed to drive the machine with a DSP control board. The phase voltages and currents are measured by high precision, high bandwidth voltage and current probes, respectively and the data are recorded in an oscilloscope (LeCroy HDO6054). The inverter input power and the electrical power of one 3-phase set alone with the mechanical power are measured by high precision power analyzer (Yokogawa WT3000). Thermocouples are inserted in the slots and end windings to measure winding temperatures and the coolant flowrate is set as 7 Litre/min by the oil cooling machine. During tests, the ambient temperature is controlled by an air conditioner as 20℃ and the winding temperatures are between 70℃ and 90℃.

A. Back Emf Test

First, the phase back emfs were measured at the base speed 4000rpm and the results are compared with the predicted values in Fig. 20. It is well-known that the magnetic property of the Cobalt steel is sensitive to manufacturing process hence the BH curve of the stator stack was measured. In addition, assembly gaps also exist between the magnets and rotor core, and they are quantified based on the manufacture tolerance. Thus, the predictions are refined with due account of these factors. In order to predict the machine behavior with stator skew, the flux and torque tables against the current and rotor angle have been produced in 2D FEA. Then, the skewed machine performance

is predicted by using the technique in [39]. For simplicity, only the measured and predicted back emfs of set ABC are plotted. It can be observed that the two waveforms match very well. Owing to the stator skew, the tooth ripple harmonics in the back emfs are eliminated and the total harmonic distortion is much lower compared with those in Fig. 5. Since the machine is configured as 3x3-phase machine, symmetry of the three 3-phase sets is examined in Fig. 21. The line-to-line back emfs of the three sets essentially overlap, which confirms the good symmetry between them. It is worth noting that the two line-to-line back emfs in Fig. 21 were measured separately.
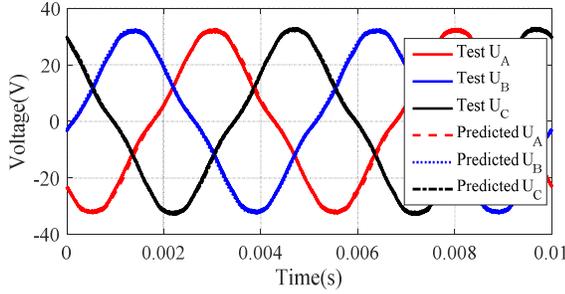

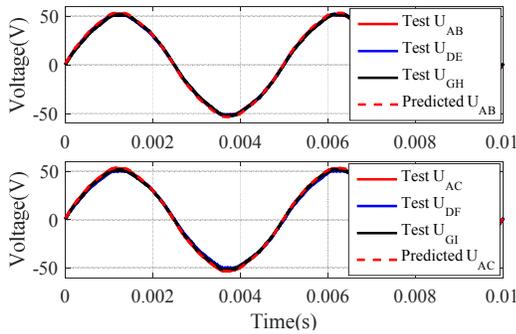Fig. 20. Phase back emf waveform comparison at 4000rpm.

Fig. 21. Line-to-line back emf waveform comparisons at 4000rpm.

B. Load Test in Healthy Operation

Load tests were carried out with the DSP based 9-phase inverter configured as three 3-phase inverters. Each 3-phase winding set is independently controlled by employing field oriented control scheme. Optimal γ angle for MTPA operation at a given current magnitude is identified by varying the current vector angle. Fig. 22 shows the measured 9 phase currents at the base speed when the reference current magnitude is 120A and the optimal γ angle is 51°. It is seen that the phase currents are well controlled with good symmetry between the three 3-phase sets. Fig. 23 compares the measured and predicted torque variations with current. The measured torque is ~5% lower than the predicted values in the worst case. This is attributed to measurement error, prediction error and frictional torque not accounted for in the prediction.
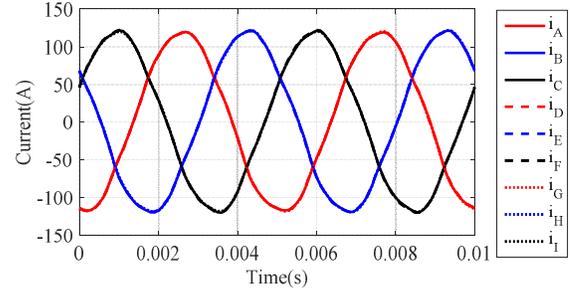

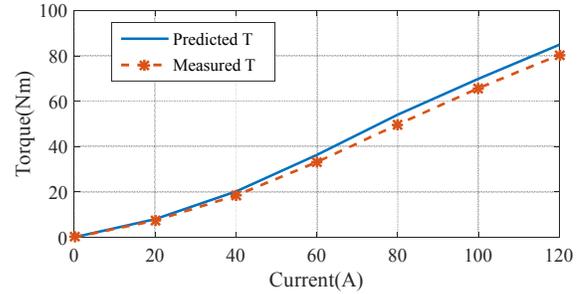Fig. 22. Phase currents at 4000rpm in healthy condition.

Fig. 23. Torque comparison in healthy condition.

C. Load Test under One 3-phase Set in Open Circuit

The prototype drive system has been tested under one 3-phase set in open circuit. During the test, 3-phase set ABC was open-circuited by switching off all the IGBTs and the remaining 3-phase sets, DEF and GHI, were controlled independently with the same reference currents, 120A in magnitude with 51° γ angle, in the healthy condition. The current waveform at the base speed is shown in Fig. 24. As can be seen, the phase currents are no longer well-balanced, and noticeable distortion are present. In addition, the phase currents of the DEF and GHI sets are also not exactly the same. These are caused by the magnetic coupling between the open-circuited set and the healthy sets, and limited current control bandwidth. The measured torque variation with current magnitude under the open circuit is compared in Fig. 25 with that in healthy condition. It can be seen that the machine is capable of providing 57.5% torque of the healthy condition with rated currents.
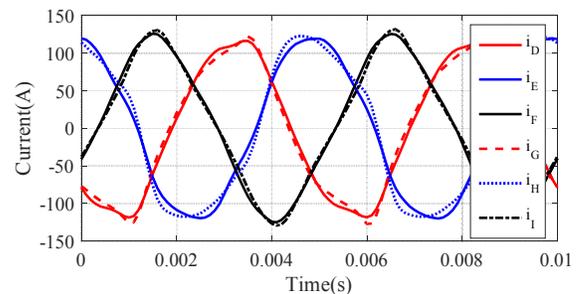

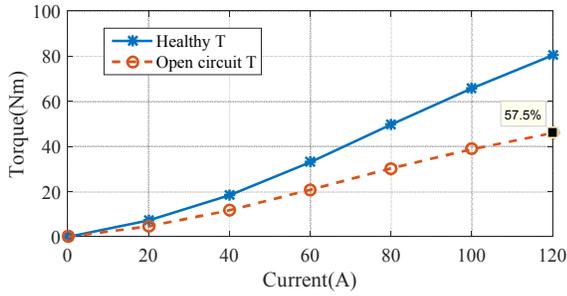Fig. 24. Healthy phase currents at 4000rpm with set ABC open circuited.

Fig. 25. Torque comparison with set ABC open circuited.

Fig. 28. Torque comparison with set ABC short circuited.

D. Load Tests under One 3-phase Set in Short Circuit

The machine drive system was also tested under one 3-phase set ABC in short circuit while the remaining 3-phase sets, DEF and GHI, were controlled independently with the same reference currents in the healthy condition stated previously. The terminal short-circuit was made by turning on all three bottom switches of the inverter as a remedy action in the event of a switch or turn-to-turn short circuit. Fig. 26 shows the short circuit currents in the fault ABC set. The currents are lower than the predictions shown in Fig. 13 because there are several volts of voltage drop on the IGBTs and addition cable impedance which were not account in the predictions. The RMS values of the short circuit currents are much lower than the rated. Hence the machine drive can cope with the short circuit fault without any thermal risk. Fig. 27 shows the phase currents in the healthy 3-phase sets where small unbalance and distortion in the waveforms due to the magnetic coupling between the healthy and faulty sets are observed. Fig. 28 compares the measured torque variation under the short circuit condition with that in the healthy condition. The torque under the ABC set short circuit condition is close to 2/3 of the torque in the healthy condition. Thus, the proposed machine drive system can tolerate the short circuit fault and output 2/3 torque with the remaining two healthy sets.
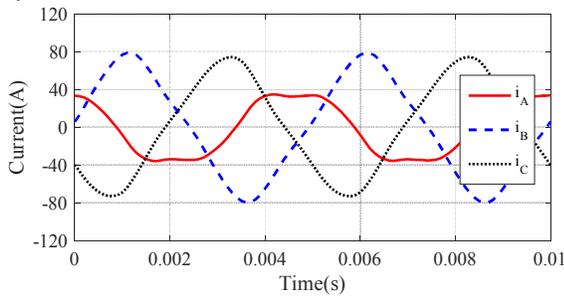

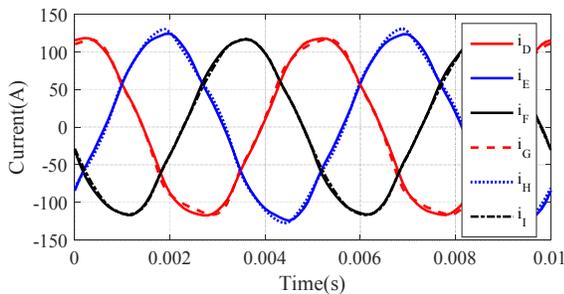Fig. 26. Short circuit phase currents at 4000rpm.

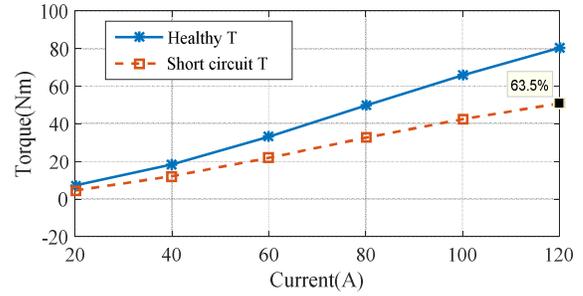Fig. 27. Healthy phase currents at 4000rpm with set ABC short circuited.

E. Thermal Tests

Thermal tests have been performed under healthy condition and one set short circuit with the rated current excitation at the base speed. One set open circuit case is not tested since the total losses, and hence the heating effect, are lower than that of the short circuit condition.

In healthy condition, the variations of the temperatures in the oil inlet, oil outlet and windings are shown in Fig. 29 when the ambient temperature is controlled to be at 20 °C. Due to the limited capacity of the heat exchanger, the temperatures of the oil inlet and outlet are not constant and increase from 24°C to 44°C and from 25°C to 57°C, respectively. The temperature rise of the three 3-phase sets should be similar due to the same load current in the healthy operation. It is noticed that the temperatures in the slots, i.e. in phases B and E slots are quite close. However, the temperature in the end winding of set DEF is 11 degrees higher than that of set ABC at steady state. This can be attributed to the loss caused by the neutral connection. For set ABC, the neutral is connected outside of the machine for easy access while the neutral of DEF is terminated in the end winding region. The neutral connection is made by soldering the three phase terminals which leads to additional resistance and loss. Since the corresponding thermocouple is placed close to the neutral point of set DEF, a higher temperature rise would be expected in set DEF end winding region.

Fig. 29. Thermal test results with 120A at 4000rpm in healthy condition.

In one set short circuit condition, the resultant temperatures are shown in Fig. 30. The temperatures of set ABC where the short circuit occurs are lower than that of set DEF in both the slot and end winding region. This is because the short circuit phase currents in set ABC are much lower than 120A as can be seen in Fig. 26. And, the temperatures of set DEF are even lower than that of healthy condition as in Fig. 29 due to fewer losses. Thus, the tests confirm the machine can operate in one

set short circuit condition without any thermal risk.

Fig. 30. Thermal test results under one set short circuit condition with 120A at 4000rpm.

The turn-to-turn fault mode has also been tested but the results are not included due to the length limit.

VI. Conclusion

In this paper, a fault tolerant machine drive based on PMA SynRM with segregated windings has been described and a prototype machine with triple redundancy has been optimally designed and built. Its performance in healthy and various faulty conditions are evaluated by FE simulations and validated by extensive experimental tests. The results show t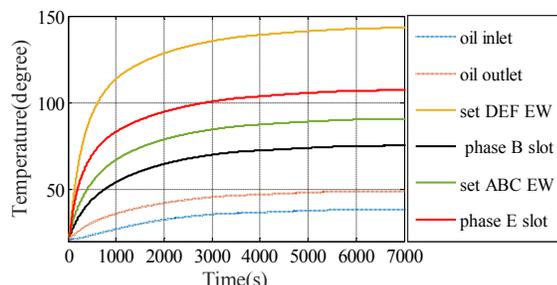hat the proposed machine exhibits excellent performance in healthy conditions and good fault tolerant capability under various fault scenarios when appropriate remedial actions are implemented. In addition, the machine can be designed without any penalties, achieving both high performance and fault tolerant capability. The proposed winding segregation scheme is also applicable to synchronous reluctance machines, synchronous wound field machines and induction machines for safety critical applications.

VII. References

[1] A. Boglietti, A. Cavagnino, A. Tenconi, and S. Vaschetto, "The safety critical electric machines and drives in the more electric aircraft: A survey," in *Industrial Electronics, 2009. IECON '09. 35th Annual Conference of IEEE*, 2009, pp. 2587-2594.

[2] J. Yu-Seok, S. Seung-Ki, S. E. Schulz, and N. R. Patel, "Fault detection and fault-tolerant control of interior permanent-magnet motor drive system for electric vehicle," *Industry Applications, IEEE Transactions on,* vol. 41, pp. 46-51, 2005.

[3] W. Cao, B. C. Mecrow, G. J. Atkinson, J. W. Bennett, and D. J. Atkinson, "Overview of Electric Motor Technologies Used for More Electric Aircraft (MEA)," *Industrial Electronics, IEEE Transactions on,* vol. 59, pp. 3523-3531, 2012.

[4] B. Vaseghi, N. Takorabet, J. P. Caron, B. Nahid-Mobarakeh, F. Meibody-Tabar, and G. Humbert, "Study of Different Architectures of Fault-Tolerant Actuator Using a Two-Channel PM Motor," *Industry Applications, IEEE Transactions on,* vol. 47, pp. 47-54, 2011.

[5] N. Bianchi and S. Bolognani, "Design of a Fault-tolerant IPM Motor for Electric Power Steering," in *Power Electronics Specialists Conference, 2005. PESC '05. IEEE 36th*, 2005, p. 2873.

[6] M. Beltrao de Rossiter Correa, C. B. Jacobina, E. R. Cabral da Silva, and A. M. N. Lima, "An induction motor drive system with improved fault tolerance," *Industry Applications, IEEE Transactions on,* vol. 37, pp. 873-879, 2001.

[7] N. Bianchi, S. Bolognani, Pre, x, M. D., and E. Fornasiero, "Post-fault operations of five-phase motor using a full-bridge inverter," in *Power Electronics Specialists Conference, 2008. PESC 2008. IEEE*, 2008, pp. 2528-2534.

[8] M. Bermudez, I. Gonzalez-Prieto, F. Barrero, H. Guzman, M. J. Duran, and X. Kestelyn, "Open-Phase Fault-Tolerant Direct Torque Control Technique for Five-Phase Induction Motor Drives," *IEEE Transactions on Industrial Electronics,* vol. 64, pp. 902-911, 2017.

[9] J.-R. Fu and T. A. Lipo, "Disturbance-free operation of a multiphase current-regulated motor drive with an opened phase," *Industry Applications, IEEE Transactions on,* vol. 30, pp. 1267-1274, 1994.

[10] L. Parsa and H. A. Toliyat, "Fault-Tolerant Interior-Permanent-Magnet Machines for Hybrid Electric Vehicle Applications," *Vehicular Technology, IEEE Transactions on,* vol. 56, pp. 1546-1552, 2007.

[11] E. Levi, R. Bojoi, F. Profumo, H. A. Toliyat, and S. Williamson, "Multiphase induction motor drives - a technology status review," *Electric Power Applications, IET,* vol. 1, pp. 489-516, 2007.

[12] Y. Fan, W. Zhu, X. Zhang, M. Cheng, and K. T. Chau, "Research on a Single Phase-Loss Fault-Tolerant Control Strategy for a New Flux-Modulated Permanent-Magnet Compact In-Wheel Motor," *IEEE Transactions on Energy Conversion,* vol. PP, pp. 1-9, 2016.

[13] M. J. Duran, I. G. Prieto, M. Bermudez, F. Barrero, H. Guzman, and M. R. Arahal, "Optimal Fault-Tolerant Control of Six-Phase Induction Motor Drives With Parallel Converters," *IEEE Transactions on Industrial Electronics,* vol. 63, pp. 629-640, 2016.

[14] J. Wang, K. Atallah, and D. Howe, "Optimal torque control of fault-tolerant permanent magnet brushless machines," *Magnetics, IEEE Transactions on,* vol. 39, pp. 2962-2964, 2003.

[15] S. Dwari, L. Parsa, and T. A. Lipo, "Optimum Control of a Five-phase Integrated Modular Permanent Magnet Motor Under Normal and Open-Circuit Fault Conditions," in *Power Electronics Specialists Conference, 2007. PESC 2007. IEEE*, 2007, pp. 1639-1644.

[16] N. Bianchi, S. Bolognani, Pre, x, and M. D., "Strategies for the Fault-Tolerant Current Control of a Five-Phase Permanent-Magnet Motor," *Industry Applications, IEEE Transactions on,* vol. 43, pp. 960-970, 2007.

[17] H. Zhou, W. Zhao, G. Liu, R. Cheng, and Y. Xie, "Remedial Field-Oriented Control of Five-Phase Fault-Tolerant Permanent-Magnet Motor by Using Reduced-Order Transformation Matrices," *IEEE Transactions on Industrial Electronics,* vol. 64, pp. 169-178, 2017.

[18] S. Gopalakrishnan, A. M. Omekanda, and B. Lequesne, "Classification and remediation of electrical faults in the switched reluctance drive," *Industry Applications, IEEE Transactions on,* vol. 42, pp. 479-486, 2006.

[19] Y. Hu, C. Gan, W. Cao, W. Li, and S. J. Finney, "Central-Tapped Node Linked Modular Fault-Tolerance Topology for SRM Applications," *IEEE Transactions on Power Electronics,* vol. 31, pp. 1541-1554, 2016.

[20] B. Lequesne, S. Gopalakrishnan, and A. M. Omekanda, "Winding short circuits in the switched reluctance drive," *Industry Applications, IEEE Transactions on,* vol. 41, pp. 1178-1184, 2005.

[21] B. C. Mecrow, A. G. Jack, J. A. Haylock, and J. Coles, "Fault-tolerant permanent magnet machine drives," *Electric Power Applications, IEE Proceedings -,* vol. 143, pp. 437-442, 1996.

[22] J. T. Chen and Z. Q. Zhu, "Comparison of All- and Alternate-Poles-Wound Flux-Switching PM Machines Having Different Stator and Rotor Pole Numbers," *Industry Applications, IEEE Transactions on,* vol. 46, pp. 1406-1415, 2010.

[23] J. Dusek, P. Arumugam, C. Brunson, E. K. Amankwah, T. Hamiti, and C. Gerada, "Impact of Slot/Pole Combination on Inter-Turn Short-Circuit Current in Fault-Tolerant Permanent Magnet Machines," *IEEE Transactions on Magnetics,* vol. 52, pp. 1-9, 2016.

[24] S. H. Han, T. M. Jahns, M. Aydin, M. K. Guven, and W. L. Soong, "Impact of Maximum Back-EMF Limits on the Performance Characteristics of Interior Permanent Magnet Synchronous Machines," in *Conference Record of the 2006 IEEE Industry Applications Conference Forty-First IAS Annual Meeting*, 2006, pp. 1962-1969.

[25] J. Wang, K. Atallah, R. Chin, W. M. Arshad, and H. Lendenmann, "Rotor Eddy-Current Loss in Permanent-Magnet Brushless AC Machines," *Magnetics, IEEE Transactions on,* vol. 46, pp. 2701-2707, 2010.

[26] M. Ferrari, N. Bianchi, A. Doria, and E. Fornasiero, "Design of Synchronous Reluctance Motor for Hybrid Electric Vehicles," *Industry Applications, IEEE Transactions on,* vol. 51, pp. 3030-3040, 2015.

[27] P. Guglielmi, N. G. Giraudo, G. M. Pellegrino, and A. Vagati, "P.M. assisted synchronous reluctance drive for minimal hybrid application," in *Industry Applications Conference, 2004. 39th IAS Annual Meeting. Conference Record of the 2004 IEEE*, 2004, pp. 1-306.

[28] Q. Dinyu, L. Xiaogang, and T. A. Lipo, "Reluctance motor control for fault-tolerant capability," in *Electric Machines and Drives Conference Record, 1997. IEEE International*, 1997, pp. WA1/1.1-WA1/1.6.

[29] B. A. Welchko, T. M. Jahns, W. L. Soong, and J. M. Nagashima, "IPM synchronous machine drive response to symmetrical and asymmetrical

short circuit faults," *Energy Conversion, IEEE Transactions on,* vol. 18, pp. 291-298, 2003.

[30] B. A. Welchko, T. M. Jahns, and S. Hiti, "IPM synchronous machine drive response to a single-phase open circuit fault," *Power Electronics, IEEE Transactions on,* vol. 17, pp. 764-771, 2002.

[31] B. Wang, J. Wang, and A. Griffo, "A Fault Tolerant Machine Drive Based on Permanent Magnet Assisted Synchronous Reluctance Machine " in *Energy Conversion Congress and Exposition (ECCE), 2016 IEEE,* Milwaukee, WI, 2016, pp. 1-8.

[32] O. V. Thorsen and M. Dalva, "A survey of faults on induction motors in offshore oil industry, petrochemical industry, gas terminals and oil refineries," in *Petroleum and Chemical Industry Conference, 1994. Record of Conference Papers., Institute of Electrical and Electronics Engineers Incorporated Industry Applications Society 41st Annual,* 1994, pp. 1-9.

[33] J. Wang, V. I. Patel, and W. Wang, "Fractional-Slot Permanent Magnet Brushless Machines with Low Space Harmonic Contents," *Magnetics, IEEE Transactions on,* vol. 50, pp. 1-9, 2014.

[34] L. Alberti and N. Bianchi, "Experimental Tests of Dual Three-Phase Induction Motor Under Faulty Operating Condition," *Industrial Electronics, IEEE Transactions on,* vol. 59, pp. 2041-2048, 2012.

[35] M. Palmieri, M. Perta, F. Cupertino, and G. Pellegrino, "High-speed scalability of synchronous reluctance machines considering different lamination materials," in *IECON 2014 - 40th Annual Conference of the IEEE Industrial Electronics Society*, 2014, pp. 614-620.

[36] P. Lazari, J. Wang, and L. Chen, "A Computationally Efficient Design Technique for Electric-Vehicle Traction Machines," *Industry Applications, IEEE Transactions on,* vol. 50, pp. 3203-3213, 2014.

[37] L. Chen, J. Wang, P. Lazari, and X. Chen, "Optimizations of a permanent magnet machine targeting different driving cycles for electric vehicles," in *Electric Machines & Drives Conference (IEMDC), 2013 IEEE International*, 2013, pp. 855-862.

[38] Q. Chen, G. Liu, W. Zhao, L. Sun, M. Shao, and Z. Liu, "Design and Comparison of Two Fault-Tolerant Interior-Permanent-Magnet Motors," *IEEE Transactions on Industrial Electronics,* vol. 61, pp. 6615-6623, 2014.

[39] P. Lazari, B. Sen, J. Wang, and X. Chen, "Accurate d and q Axis Modeling of Synchronous Machines With Skew Accounting for Saturation," *IEEE Transactions on Magnetics,* vol. 50, pp. 1-4, 2014.

Bhaskar Sen (M'17) received the B.E. degree from the Delhi College of Engineering, Delhi, India, in 2003, the M.Tech. degree from the Indian Institute of Technology, Kanpur, India, in 2006, both in electrical engineering, and the Ph.D. degree in electrical and electronic engineering from The University of Sheffield, Sheffield, U.K., in 2015. From 2006 to 2011, he was a Research Engineer with GE Global Research, Bangalore, India. From 2015 to 2017, he was a Research Associate at The University of Sheffield. His research interests include electrical machine fault modeling, machine fault detection, and fault-tolerant drives.

Antonio Griffo (M'13) received the M.Sc. degree in electronic engineering and the Ph.D. degree in electrical engineering from the University of Napoli "Federico II," Naples, Italy, in 2003 and 2007, respectively. From 2007 to 2013, he was a Research Associate with the University of Sheffield, Sheffield, U.K., and the University of Bristol, Bristol, U.K. He is currently a Lecturer with the Department of Electronic and Electrical Engineering, University of Sheffield. His research interests include modeling, control and condition monitoring of electric power systems, power electronics converters, and electrical motor drives, for renewable energy, automotive and aerospace applications.

Zhigang Sun received his PhD degree in Electrical Engineering from the University of Sheffield in 2009. He has been working in the field of electrical power systems in various professional roles in aerospace industry, semiconductor industry and higher education since 2009. He is currently an Electrical Engineer at Rolls-Royce Electrical.

Ellis Chong received the Ph.D. degree in electrical engineering from the University of Cambridge, the U.K., in 2001.

He is a Chartered Electrical Engineer and has been working in the Aerospace, Marine and Power Engineering sectors in the areas of electrical machines and power electronics since 2001. He is currently the UK Chief Design Engineer with the Rolls-Royce Electrical Group, Rolls-Royce Plc, Derby, U.K.

Bo Wang (M'17) received the B.Eng. and M.Sc. degrees in electrical engineering from Nanjing University of Aeronautics and Astronautics, Nanjing, China, in 2009 and 2012, respectively.

From 2012 to 2014, he served as a senior engineer in the Delta Electronics Co. Ltd. Since 2014, he has been working toward the Ph.D. degree at the Department of Electronic and Electrical Engineering, University of Sheffield, Sheffield, U.K., where he is working as a research associate. His research interests include the permanent magnet machine drives, electric traction and fault tolerant systems.

Jiabin Wang (SM'03) received the B.Eng. and M.Eng. degrees from Jiangsu University, Zhengjiang, China, in 1982 and 1986, respectively, and the Ph.D. degree from the University of East London, London, U.K., in 1996, all in electrical and electronic engineering.

Currently, he is a Professor in Electrical Engineering at the University of Sheffield, Sheffield, U.K. From 1986 to 1991, he was with the Department of Electrical Engineering at Jiangsu University, where he was appointed a Lecturer in 1987 and an Associated Professor in 1990. He was a Postdoctoral Research Associate at the University of Sheffield, Sheffield, U.K., from 1996 to 1997, and a Senior Lecturer at the University of East London from 1998 to 2001. His research interests range from motion control and electromechanical energy conversion to electric drives for applications in automotive, renewable energy, household appliances and aerospace sectors.
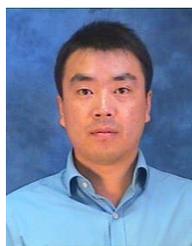
He is a fellow of the IET and a senior member of IEEE.